The Nitriding Kinetics of Iron-Chromium Alloys; The Role of Excess Nitrogen: Experiments and Modelling

R.E. SCHACHERL, P.C.J. GRAAT, and E.J. MITTEMEIJER

To investigate the morphology and the growth kinetics of nitrided layers of Fe-Cr alloys, nitriding experiments were performed for alloys with 4.3, 7.7, 14.0, and 21.5 at. pct Cr. The precipitation morphology of the nitrided samples was investigated with light optical microscopy and scanning electron microscopy (SEM). The elemental compositional variation was determined with electron probe microanalysis. To describe the evolution of the thickness of the nitrided layers, a numerical model was developed that has as important (fit) parameters: the surface nitrogen content, the solubility product of chromium and nitrogen dissolved in the ferrite matrix, and a parameter defining the composition of the precipitated chromium nitride. Fitting of the model to the experimental data demonstrated for the first time that mobile and immobile excess nitrogen is present in the nitrided layers and that the mobile excess nitrogen considerably influences the nitriding rate.

I. INTRODUCTION

NITRIDING of iron-based alloys is a process that can lead to pronounced improvement of the fatigue, corrosion, and wear properties of workpieces in countless practical applications.[1] To optimize the properties obtained, the growth kinetics of the surface adjacent nitrided zone, *i.e.*, the thickness increase as dependent on the applied nitriding parameters (time, temperature, nitriding potential, and specimen composition) has to be known.

If pure iron is nitrided, three different Fe-N phases can occur successively:[2] α-Fe [N] (ferrite) with a bcc structure, where the nitrogen is statistically distributed over the octahedral interstitial sites of the bcc Fe–sublattice; the γ'-Fe$_4$N$_{1-x}$ phase based on an fcc Fe sublattice, where the nitrogen atoms are distributed in an ordered way over the octahedral interstitial sites; and the ε-Fe$_2$N$_{1-x}$ phase based on an hcp Fe sublattice, where the nitrogen atoms are distributed over the octahedral interstitial sites in a more or less ordered way. The amount of nitrogen dissolved in iron depends on the nitriding temperature and the chemical potential of nitrogen in the nitriding atmosphere, which in the case of gaseous nitriding can be adjusted by varying the composition of the mixture of the ammonia and the hydrogen in the gas phase.[3,4,5] If the nitriding conditions allow the formation of ε, it will be formed at the surface. As a second layer, γ' will be formed below the ε layer. The surface layer containing the γ' and the ε phases (sublayers) is called the "compound layer." The last "layer," underneath γ', the so-called "diffusion zone," consists of α-Fe (the original substrate) where the nitrogen atoms are dissolved interstitially (previously, discussed).[5–9]

If the iron matrix (substrate) contains alloying elements with a relatively high affinity for N, nitrides of these elements can be formed during nitriding and these thus occur in the diffusion zone. Chromium is often used as an alloying element in nitriding steels, because of the relatively strong Cr-N interaction,[10,11,12] which allows the formation of chromium nitride.[13,14] Experimentally determined and theoretically calculated sections at constant temperature of the ternary phase diagram Fe-Cr-N are given in References 15 and 16. Such results pertaining to the relatively low temperatures and high nitriding potentials (corresponding to about 3100 atm) used in this work are not available.

During the nitriding process, the formation of chromium nitride proceeds by nucleation and growth. In the initial stage, very small coherent precipitates develop. This stage is associated with a relatively high hardness, caused by the strain fields, which are induced by the misfit between the CrN particles and the α-Fe matrix.[14] Continued nitriding involves aging for the CrN particles already formed and left behind in the wake of the migrating reaction front. This aging process leads to coarsening of these CrN precipitates, in association with loss of coherency, corresponding with a decrease of misfit strain energy and a decrease of α-Fe/CrN interfacial area.[14] The coarsening process can occur as so-called "continuous coarsening" involving growth of larger particles at the cost of smaller particles or as "discontinuous coarsening" (*cf.* terminology given in Reference 17) involving development of a lamellar structure of CrN and α-Fe.[14,18–23] Both coarsening reactions can occur simultaneously and lead to a decrease of hardness, which is most pronounced for the lamellar microstructure.[14] A peculiar and important (discussed subsequently) observation is the occurrence of so-called excess nitrogen: enhanced uptake of nitrogen in the nitrided zone, ascribed to the nitride-precipitate/matrix misfit-strain field.[12,14]

Obviously, with a view to practice, model descriptions for the kinetics (*i.e.*, time and temperature dependencies) of (ε/γ') nitride layer growth and diffusion zone growth are needed. A satisfactory approach for modeling (bi)layer (nitride) growth (*i.e.*, compound layer growth) upon nitriding iron exists.[5,6] For describing the growth of the diffusion zone under simultaneous development of alloying-element nitrides, a satisfactory,

generally valid model has not been presented until now (also discussed in Section II). According to the present authors, this may be due to the ignorance of the role of the so-called excess nitrogen (*cf.* previous discussion) on nitriding kinetics. This work presents a general model for the description of the nitriding kinetics of iron-based alloys, incorporating the excess nitrogen (Section II). The model allows distinction between the effects of "mobile" and "immobile" excess nitrogen and has been applied successfully to Fe-Cr alloys subjected to gaseous nitriding (Section IV).

II. MODEL FOR THE KINETICS OF DIFFUSION ZONE GROWTH

Consider an Fe-Me alloy that is nitrided employing a nitriding potential such that no iron nitrides can be formed at the surface, but upon nitriding, a diffusion zone containing MeN_n nitride particles develops.

The first proposals to describe diffusion zone growth upon nitriding have been derived from a simple model originally meant for "internal oxidation".[24] The following assumptions have to be made for this model, if it is applied to "inner nitriding":[14,24]

(1) The nitrogen dissolved in the ferrite matrix (α) exhibits Henrian behavior. This implies that the diffusion coefficient of nitrogen in the ferrite matrix is independent of the dissolved nitrogen content.
(2) The reaction of dissolved nitrogen with dissolved Me, leading to the nitride MeN_n, takes place only and completely at a sharp interface between the nitrided zone and the not nitrided core.
(3) The amount of nitrogen required for building up the concentration profile in the ferrite matrix of the nitrided zone is negligible in comparison to the amount of nitrogen that is consumed at the reaction interface.
(4) Diffusion of Me can be neglected and is not nitriding-rate determining.
(5) Nitrogen is taken up rapidly from the nitriding medium/ specimen surface, so that the surface concentration $c_{N_\alpha}^s$ is equal to the lattice solubility of nitrogen, corresponding to the chemical potential of nitrogen in the nitriding atmosphere.

With these assumptions and approximating the concentration gradient of dissolved nitrogen with $-c_{N_\alpha}^s/z$, the amount of nitrogen (per unit area) that reaches the reaction front in the time period dt is equal to $(c_{N_\alpha}^s \cdot D_N/z)dt$, where z is the depth coordinate of the reaction front. This nitrogen amount must equal the nitrogen amount required to move the reaction front a distance dz, *i.e.*, $n \cdot c_{Me} \cdot dz$, where c_{Me} is the Me concentration. Upon integration of the resulting differential equation for constant temperature, Eq. [1] is obtained:

$$z^2 = \left(\frac{2 \cdot c_{N_\alpha}^s \cdot D_N}{n \cdot c_{Me}} \right) \cdot t \qquad [1]$$

Hence, at constant temperature, a parabolic relation should occur between the nitriding time and the thickness of the nitrided layer.

This model has been often used to predict the case depth of the nitrided zone.[14,19,25] A major simplification introduced in applying the model is that the solubility of nitrogen in the ferrite matrix is taken as that pertaining to unstrained, pure α-Fe; excess nitrogen dissolved in the α-Fe matrix is not considered.

Excess nitrogen is the amount of nitrogen that exceeds the "normal" capacity of nitrogen uptake. This normal capacity for nitrogen uptake consists in the case of a Fe-Me alloy of

(1) the amount of nitrogen dissolved interstitially in the unstrained α-Fe matrix, and
(2) the amount of nitrogen that is incorporated in the MeN_n precipitates.

The difference between the total amount of nitrogen in the nitrided zone and this normal capacity is defined as "excess" nitrogen. Three types of excess nitrogen are distinguished: (1) nitrogen that is trapped at dislocations (in particular for deformed alloys[26]), (2) nitrogen that is adsorbed at matrix/ precipitate interfaces, and (3) nitrogen that is (additionally) dissolved in the strained α-Fe matrix. Such excess nitrogen was found in nitrided Fe-Ti,[27,28,29] Fe-V,[30] Fe-Mo,[30] Fe-Al,[26,31] and Fe-Cr alloys.[14,23,32]

With a view to the nitriding kinetics, the effects of the various kinds of excess nitrogen will be different. It is proposed here to distinguish between mobile excess nitrogen, *i.e.*, nitrogen dissolved in the ferrite lattice, and immobile excess nitrogen, *i.e.*, nitrogen trapped at dislocations and adsorbed at the nitride/matrix interfaces. Mobile excess nitrogen will enhance the extent of the diffusion zone, whereas immobile excess nitrogen will decrease the extent of the nitrided zone. This becomes immediately clear, already on inspection of the simple Eq. [1]: mobile excess nitrogen expresses itself by an increase of the lattice solubility $c_{N_\alpha}^s$; immobile excess nitrogen may be effectively expressed by an increase of the stoichiometric parameter n. However, to avoid the crude simplifications inherent to application of Eq. [1], in this article, the following numerical model is proposed to incorporate the effects of immobile and mobile excess nitrogen on nitriding kinetics.

The inward diffusion of nitrogen in the α-Fe matrix can be described with Fick's second law:

$$\frac{\partial c_{N_\alpha}(z, t)}{\partial t} = D_N \cdot \frac{\partial^2 c_{N_\alpha}(z, t)}{\partial z^2} \qquad [2]$$

where $c_{N_\alpha}(z,t)$ is the nitrogen dissolved in the α-Fe matrix at depth z at time t and at temperature T. The term D_N is the diffusion coefficient of nitrogen in α-Fe, which can be taken as concentration independent.[5,6] The formation of nitrides of possibly present alloying elements removes dissolved, mobile nitrogen from the matrix; nitrogen then is trapped as immobile nitrogen in the nitrides formed. The formation of MeN_n can be expressed with the following equation:

$$Me_\alpha + nN_\alpha \Leftrightarrow MeN_n \qquad [3]$$

where Me_α and N_α denote alloying element and nitrogen dissolved in the α-Fe matrix. The equilibrium constant of Reaction [3], K_e, obeys

$$K_e = \frac{1}{[Me_\alpha] \cdot [N]^n} = \frac{1}{K_{MeN_n}} \text{ with } K_{MeN_n} = [Me_\alpha] \cdot [N_\alpha]^n \qquad [4]$$

where $[Me_\alpha]$ and $[N_\alpha]$ denote the concentrations of dissolved Me and dissolved N in the α-Fe matrix, and K_{MeN_n} is the

corresponding solubility product of Me_α and N_α. The precipitation of MeN_n will take place at a certain location if there it holds

$$[Me_\alpha][N_\alpha]^n > K_{MeN_n} \qquad [5]$$

In solving Fick's second law (Eq. [2]), it must be tested at every location (depth z) for every time (step) if the solubility product, K_{MeN_n}, is surpassed. If this is the case, precipitation of MeN_n, at the location considered, should be allowed for until $[Me_\alpha][N_\alpha]^n = K_{MeN_n}$. Thereby, a numerical finite difference (explicit method) solution method is naturally suggested to solve Fick's second law, subject to the prevailing boundary conditions. Thus, adopting the finite-difference approach of Reference 33, in this work, the nitrogen concentration at depth z_i and at time t_{j+1}, $c_{N_\alpha}(i, j + 1)$, is calculated from the nitrogen concentrations at the previous time t_j at the depths $i - 1$, i and $i + 1$ according to

$$c_{N_\alpha}(i, j+1) = c_{N_\alpha}(i,j) + \beta \cdot \{c_{N_\alpha}(i-1,j) - 2 \cdot c_{N_\alpha}(i,j) + c_{N_\alpha}(i+1,j)\} \qquad [6]$$

where $\beta = D_N(\Delta t/\Delta z^2)$ with Δt and Δz as time and depth steps.

The application of a solubility product constraint as indicated by Eq. [5] was earlier applied to a case of carburizing.[34,35] Attempts to apply the approach to cases of nitriding until now either ignored entirely the presence and role of excess nitrogen[36] or, erroneously, considered the excess nitrogen dissolved in the ferrite lattice as immobile, *i.e.*, not contributing to nitrogen diffusion, and ignored the presence of immobile excess nitrogen adsorbed at the nitride–particles/matrix interfaces (as previously discussed).[37]

In this work, the presence of mobile excess nitrogen is recognized by considering the nitrogen lattice solubility at the surface, $c_{N_\alpha}^s$, as a fit parameter (*i.e.*, not assume $c_{N_\alpha}^s$ equal to the equilibrium nitrogen solubility of (unstrained) ferrite). The presence of immobile excess nitrogen is recognized by replacing the stoichiometric parameter n in MeN_n by $b = n + x$, with x as the contribution of the immobile excess nitrogen. The fit parameters in the current model thus are $c_{N_\alpha}^s$, b, and K_{MeN_n}. The scheme of calculating the nitrogen concentration–depth profile, and the depth profile of the amount of MeN_n precipitates, according to the finite difference method, is shown in Figure 1. The following boundary conditions are adopted.

(1) The initial nitrogen concentration is constant and given by $c_{N_\alpha}^{t=0}$ (for $z \neq 0$): $c_{N_\alpha}(i,1) = c_{N_\alpha}^{t=0}$ for $i > 1$. In the present case, $c_{N_\alpha}^{t=0}$ is virtually zero.
(2) The surface concentration is always given by $c_{N_\alpha}^s$: $c_{N_\alpha} = (1,j) = c_{N_\alpha}^s$.
(3) There is no net flux through the center plane of the specimen (sheet) at $z = z_M$. This is realized by taking the concentrations at the grid points adjacent to the grid point at the center plane, indicated by $i = M$, equal to each other, *i.e.*, $c_{N_\alpha}(M - 1, j) = c_{N_\alpha}(M + 1, j)$. Hence (*cf.* Eq. [6]),

$$c_{N_\alpha}(M, j+1) = (1 - 2\beta)c_{N_\alpha}(M,j) + 2\beta c_{N_\alpha}(M-1,j) \quad [7]$$

On the preceding basis, the importance of incorporating the presence of both mobile and immobile excess nitrogen in the modeling of nitriding kinetics can be demonstrated by simulations (as follows).

A Fe-7 wt pct Cr alloy is considered, which is nitrided at 580 °C and a nitriding potential of $r_n = 0.1$ atm$^{-1/2}$ for
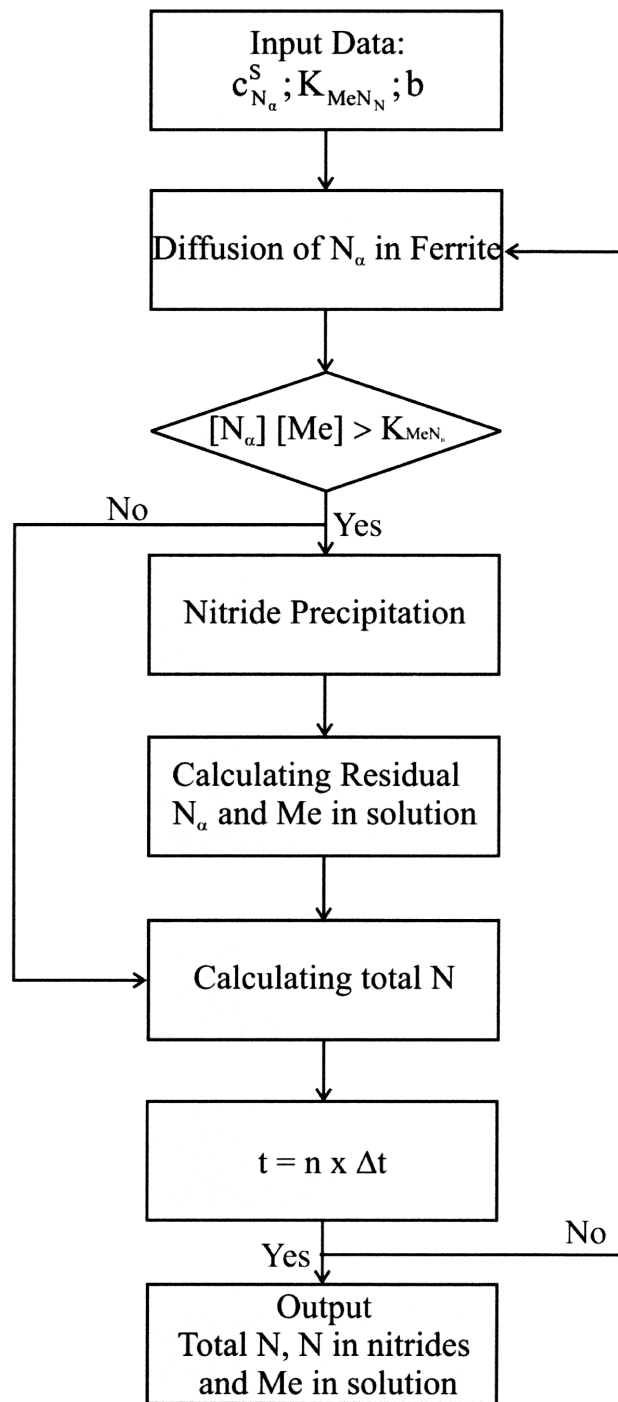

Fig. 1—Flow chart showing the scheme of calculating the nitrogen concentration and MeN_n precipitate depth profiles. Total N denotes the amount of nitrogen bound in CrN and dissolved in the ferrite matrix. The letter n in the flow chart indicates the number of time-steps.

7 hours. The solid line in Figure 2 shows the resulting nitrogen-concentration depth profile as calculated for the case that neither mobile nor immobile excess nitrogen is present in the nitrided layer. This means that (1) the surface nitrogen content $c_{N_\alpha}^s$ is equal to the solubility of nitrogen in pure, unstrained ferrite, in accordance with the applied nitriding parameters ($r_n = 0.1$ atm$^{-1/2}$, $T = 580$ °C; for data on $c_{N_\alpha}^s$, refer to References 4 and 5); and (2) that b is equal to $n = 1$ [no immobile excess nitrogen).

If only the existence of mobile excess nitrogen is assumed, which is expressed by a higher value for $c_{N_\alpha}^s$, clearly a significantly larger extent (depth) of the nitrided zone occurs (dashed line in Figure 2). If only the existence of immobile excess nitrogen is assumed, which is expressed by a value of b larger than n ($=1$ for the present case of CrN precipitation), a somewhat smaller penetration depth of nitrogen occurs (dotted line in Figure 2).

The preceding values for $c_{N_\alpha}^s$ and b are realistic values (Section IV). Evidently, the presence of mobile and immobile excess nitrogen has a pronounced influence on the nitriding kinetics. The effect of mobile and immobile excess nitrogen has to be recognized in any model that should be able to predict properties resulting from nitriding.

Another important parameter in the preceding numerical model is the equilibrium solubility product, K_{MeN_n}, which controls the (local) occurrence of precipitation. The influence of K_{CrN} on the nitrogen-depth profile is shown in Figure 3.

Relatively large K_{CrN} values imply that (at the reaction front) not all dissolved Cr reacts with nitrogen to chromium nitride and thus the extent of the nitrided zone is larger for larger K_{CrN}, although in association with a more gradual transition between the nitrided zone and the non-nitrided core of the sample.
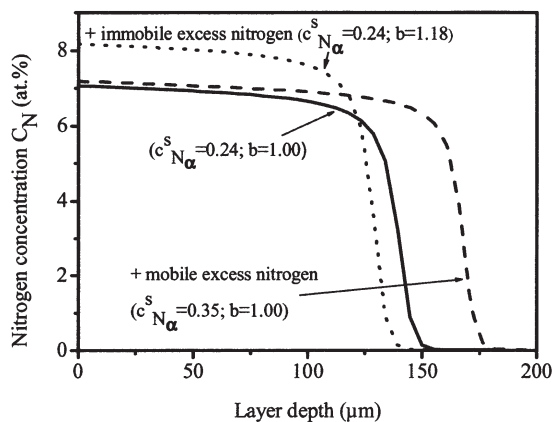

Fig. 2—Effect of mobile and immobile excess nitrogen on the development of the nitrogen concentration-depth profile. Fe-7 wt pct Cr alloy sheet nitrided at 580 °C at a nitriding potential $r_n = 0.1$ atm$^{-1/2}$.
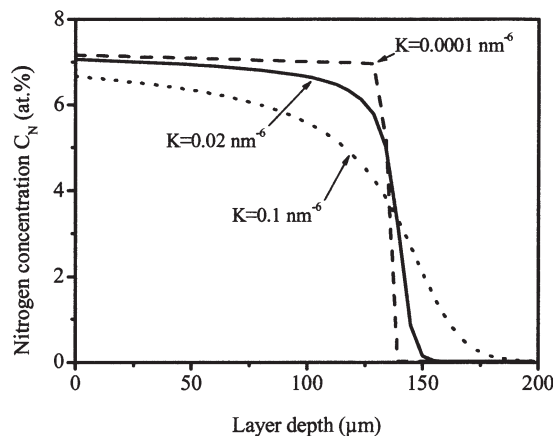

Fig. 3—Effect of the solubility product K_{MeN} (nm^{-6}) on the development of the nitrogen concentration-depth profile. Fe-7 wt pct Cr alloy sheet nitrided at 580 °C and at a nitriding potential of $r_n = 0.1$ atm$^{-1/2}$ for 7 h.

III. EXPERIMENTAL

A. Specimen Preparation

Fe-Cr alloys with nominally 4.3, 7.7, 14.0, and 21.5 at. pct Cr (coded as Fe-4Cr, Fe-7Cr, Fe-13Cr, and Fe-20Cr, respectively) were prepared from pure Fe (99.98 wt pct) and pure Cr (99.999 wt pct) in an inductive furnace under argon atmosphere (99.999 vol pct). The Cr content of the alloys was verified employing X-ray fluorescence analysis. The melt process was performed in an Al_2O_3 crucible. The amounts of oxygen, nitrogen, carbon, and sulfur impurities in the produced alloys were determined by chemical analysis (inductive-coupled plasma-optic emission spectroscopy). The average results for each alloy composition are shown in Table I. It is likely that the detected oxygen is due to the (natural) oxide layer on the specimen surface.

After casting, the alloys have cylindrical shape with a diameter of 10 mm and a length of 100 mm. The cast alloys were cold rolled to sheets with a thickness of 1.2 ± 0.1 mm. The obtained sheets were cut into rectangular pieces of lateral dimensions 1.5×1.5 mm^2. These pieces were subsequently cleaned in an ultrasonic bath filled with ethanol and encapsulated in a silica tube filled with argon (purity: 99.999 vol pct) up to a pressure of 750 Torr. The encapsulated samples were annealed for 1 hour at 700 °C (within the α-phase region of the Fe-Cr diagram) to get a recrystallized grain structure. After annealing, the grains had an average diameter of 45 μm.

Electron probe microanalysis (also discussed in Section C–4) was used to verify that Cr was distributed homogenously in the sample. Before nitriding, the samples were ground, polished (last step: 1-μm diamond paste), and cleaned in an ultrasonic bath filled with ethanol.

B. Nitriding

For nitriding, a sample was suspended at a quartz fiber in a vertical tube furnace. To start the nitriding process, the sample was placed in the middle of the nitriding furnace. The nitriding experiments were performed at 580 °C ($=853$ K) in an ammonia/hydrogen gas flux (purity: H$_2$: 99.999 vol pct, NH$_3$: $>$99.998 vol pct). The fluxes of both gases were adjusted with mass flow controllers and amounted to 9 and 91 mL/min for ammonia and hydrogen, respectively, which corresponds with a nitriding potential $r_n \equiv p_{NH_3}/p_{H_2}^2$[4] of about $r_n = 0.1$ atm$^{-1/2}$. It should be recognized that nitriding at 580 °C in this NH$_3$/H$_2$ atmosphere is equivalent to nitriding in pure N$_2$ at about 3100 atm.[4] The nitriding times for this study have been given in Table II for the investigated Fe-Cr alloys.

At the end of the nitriding process, the samples were quenched in water.

Table I. Amounts of Light Element Impurities for Each Alloy Used in This Work

Alloy	O (μg/g)	N (μg/g)	C (μg/g)	S (μg/g)
Fe-4Cr	117 ± 10	<5	6 ± 2	6 ± 3
Fe-7Cr	132 ± 10	<5	63 ± 10	7 ± 3
Fe-13Cr	146 ± 10	<5	4 ± 2	5 ± 2
Fe-20Cr	155 ± 15	<5	9 ± 2	3 ± 2

Table II. Applied Nitriding Times at a Temperature of 580 °C

Fe-4Cr	0.25 h	1 h	2 h	5 h	7 h	15 h	
Fe-7Cr	1 h	4 h	5 h	7 h	10 h	15 h	20 h
Fe-13Cr	7 h	10 h	15 h	20 h	24 h	31 h	48 h
Fe-20Cr	7 h	15 h	20 h	24 h	31 h	48 h	

C. *Specimen Characterization*

1. *Microscopy*

For light microscopical investigation, pieces were cut from the samples and prepared to cross sections, by subsequent embedding (Konduktomet, Buehler* GmbH), polishing (last

*Buehler is a trademark of Buehle Ltd., Lake Bluft, USA.

step: 1-μm diamond paste) and etching with 2.5 pct nital (2.5 vol pct HNO_3 in ethanol) for about 5 seconds. These cross sections were investigated with light optical microscopy applying a Leica** DMRM microscope. The light micrographs

**Leica and Leitz are trademarks of Leica Microsystems AG, Wetzlar, Germany, Leica Camera AG, Solms, Germany and Leica Geosystems AG, Heerbrug, Switzerland.

were recorded with a digital camera (Jenoptik*** Progres 3008).

***Jenoptik is a trademark of Jenoptik AG, Jena, Germany.

For scanning electron microscopy (SEM), the same (etched) cross sections were used as for light microscopy. The SEM micrographs were taken with a JEOL**** JSM 6300F

****JEOL is a trademark of Japan Electron Optics Ltd., Tokyo.

operating at 3 or 5 kV.

2. *Hardness measurements*

Hardness measurements across the cross sections of the nitrided specimens were performed with a Leitz** Durimet hardness tester, applying a load of 50 g. The presented hardness values are average values of five measurements.

3. *X-ray diffraction*

To determine which phases are present after nitriding, X-ray diffraction (XRD) was applied using a PHILIPS***** X'Pert

*****PHILIPS is a trademark of Royal Philips, Eindhoven, The Netherlands.

diffractometer. Measurements were made using Cu K_α and Co K_α radiations and employing the Bragg–Brentano geometry with a graphite monochromator in the diffracted beam. The diffraction angle (2Θ) range scanned was 10 to 130 deg, with a step size of 0.05 deg. The X-ray diffractograms were recorded from specimen surfaces as obtained after nitriding. To identify the phases from the diffraction peaks, the data from the JCPDS data base were used.[38]

4. *Electron probe microanalysis*

To determine the composition of the nitrided zones of the samples after nitriding, electron probe microanalysis (EPMA) was performed employing a Cameca****** SX100 instrument.

******Cameca is a trademark of Cameca, CorrocVoic, France.

Cross sections of the nitrided alloys, similar to those described previously for light and scanning electron microscopy, were analyzed, but in this case, no etching after polishing was applied. A focused electron beam at an accelerating voltage of 15 kV and a current of 100 nA was applied. To obtain the element contents in the specimens, the intensity of the characteristic Fe K_β, Cr K_β, N K_α, and O K_α X-ray emission peaks was determined at points along lines across the cross sections (single measurement points at a distance of 2 μm). The intensities obtained from the nitrided samples were divided by the intensities obtained from standard samples of pure Fe (Fe K_β), pure Cr (Cr K_β), andradite/ $Ca_3Fe_2(SiO_4)_3$ (O K_α), and γ'-Fe_4N (N K_α). Concentration values were calculated from the intensity ratios applying the $\Phi(\rho z)$ approach according to Pouchou and Pichoir (PAP).[39]

IV. RESULTS AND EVALUATION

Upon nitriding, all samples show, for all nitriding times and Cr contents applied, distinct nitrogen uptake, with the exception of the Fe-20Cr alloy nitrided shorter than 5 hours at 580 °C. It was shown, contrary to practical knowledge, that even for high chromium contents (as 20 wt pct), nitriding at relatively low temperatures is possible, provided an oxygen-free atmosphere is applied.[23]

A. *Phase Analysis; XRD*

To determine the phases present in the nitrided zone, X-ray diffractograms were recorded from each nitrided sample. The diffractograms of a Fe-7Cr alloy nitrided for 20 hours at 580 °C and of a Fe-20Cr alloy nitrided for 24 hours at 580 °C are shown in Figure 4.

Clearly, after nitriding, only the ferrite (α) and CrN phases are present. As can be expected, the diffractogram of nitrided Fe-7Cr exhibits a lower intensity for the CrN peaks than the diffractogram of the nitrided Fe-20Cr. The occurrence of separate CrN diffraction peaks indicates the presence of relatively coarse CrN particles. This is consistent with the light microscopical results presented in Section B (discontinuous coarsening adjacent to the surface).

B. *Morphologies of the Nitrided Zone; Microscopical Investigation*

Light micrographs of cross sections of Fe-4Cr, Fe-7Cr, Fe-13Cr, and Fe-20Cr specimens nitrided at 580 °C for 7 hours are shown in Figure 5.

In the micrographs of the Fe-4Cr (Figure 5(a)) and Fe-7Cr (Figures 5(b) and 6) specimen, four regions (from the surface to the not nitrided core), indicated as zones I through IV in Figure 6, can be distinguished.

(1) Mainly near the surface, dark grains occur, which show a lamellar morphology in the SEM micrographs (zone I in Figure 6 and Figure 7). In this region, the CrN that has initially been formed as finely dispersed (coherent) precipitates has (already) been transformed by a discontinuous coarsening reaction into the lamellar ferrite/CrN morphology (for detailed discussion, refer to Reference 23).

(2) Below this region, bright grains with clearly visible grain boundaries are present (zone II in Figure 6). In this region,
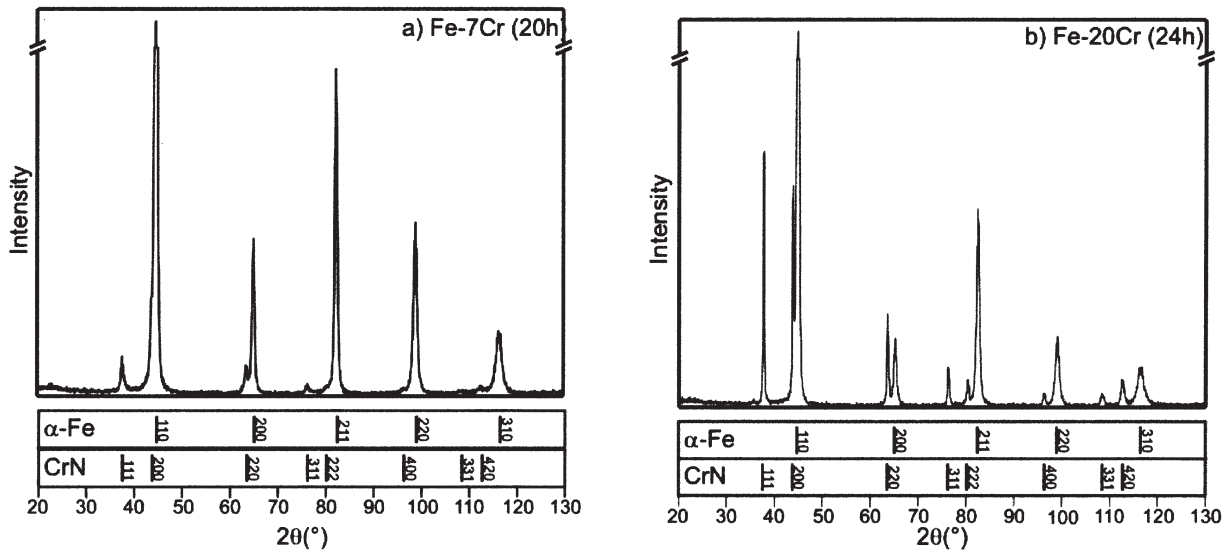
Fig. 4—XRD diffractograms of (*a*) the Fe-7Cr alloy nitrided for 20 h at 580 °C and (*b*) the Fe-20Cr alloy nitrided for 24 h at 580 °C.
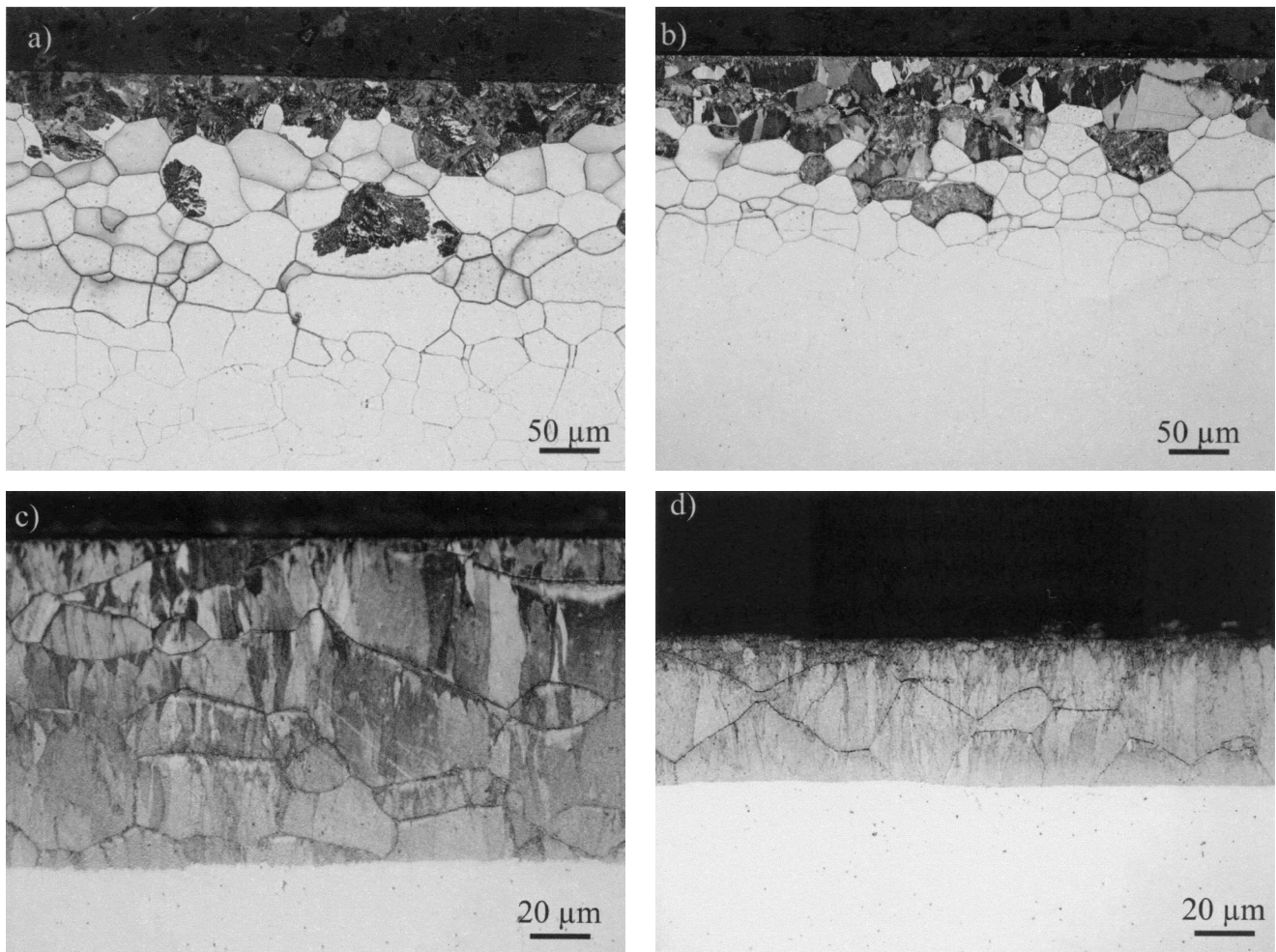

Fig. 5—Light micrographs of cross sections of the nitrided (*a*) Fe-4Cr, (*b*) Fe-7Cr, (*c*) Fe-13Cr, and (*d*) Fe-20Cr specimens. All alloys were nitrided for 7 h at 580 °C.

CrN is still present as finely dispersed submicroscopical precipitates within the grains (not visible with SEM but with transmission electron microscopy (TEM)[40]), which

is consistent with the much higher hardness (1180 HV 0.05) of these grains as compared to the dark grains (720 HV 0.05). The very pronounced visibility of the grain bound-
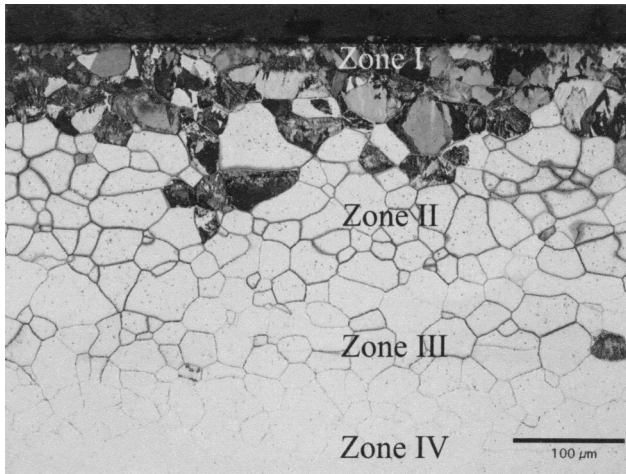
Fig. 6—Light optical micrograph of a Fe-7Cr sample nitrided at 580 °C for 20 h at a nitriding potential of 0.1 $atm^{-1/2}$. For discussion of the zones indicated, refer to Section B.
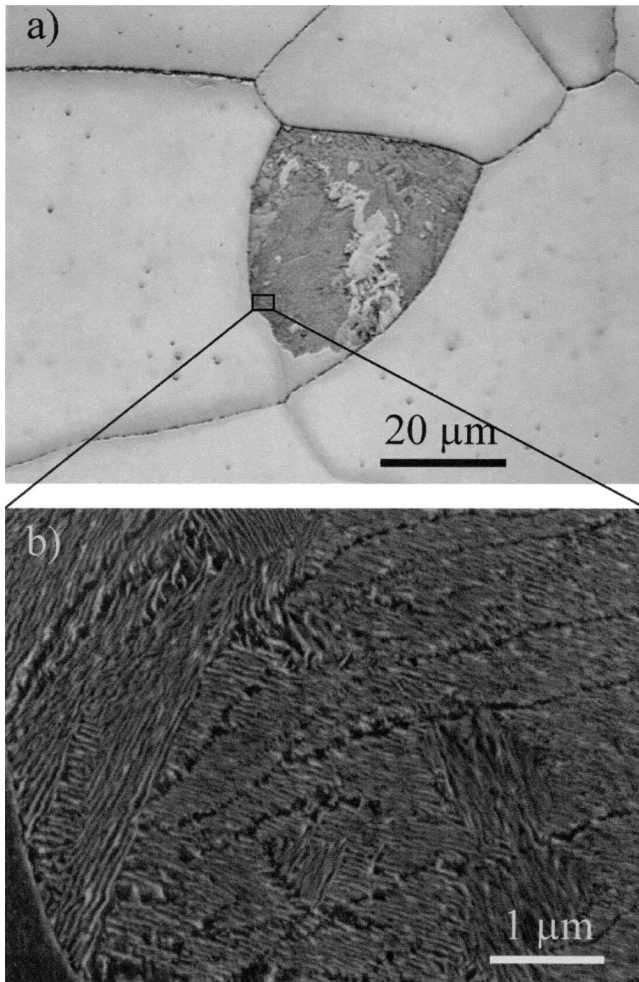

Fig. 7—An original grain of the Fe-4Cr alloy after nitriding transformed by the discontinuous coarsening reaction (5 h nitriding at 580 °C): (a) optical micrograph; and (b) SEM micrograph of the region indicated in (a). The SEM micrograph reveals the occurrence of many differently oriented colonies of lamellae.

aries is probably caused by preferential formation of CrN precipitates at the grain boundaries or the onset of discontinuous transformation at the grain boundaries.[14]

(3) At larger depths, the visibility of the grain boundaries gradually decreases (zone III in Figure 6). In this depth range, not all Cr has reacted to CrN yet.

(4) Finally, the un-nitrided core (zone IV in Figure 6) of the sample follows, where the grain boundaries are not visible anymore. In not nitrided (parts of the) specimens, etching does not clearly reveal grain boundaries because the Cr in the specimen causes a protecting Cr_2O_3 layer, preventing chemical attack by the etching agent (Figures 5(b) through (d)). Obviously, this protection is less for the alloy with low Cr content (Fe-4Cr), leading to grain boundary visibility after etching also in the not-nitrided core of this alloy (Figure 5(a)).

In the micrographs of the Fe-13Cr and Fe-20Cr specimens, only two regions can be distinguished, namely, the surface adjacent, nitrided region, which has completely been transformed by the discontinuous coarsening reaction, and the unnitrided core. The boundary between the nitrided and un-nitrided regions is relatively sharp as compared to the nitrided Fe-4Cr and Fe-7Cr specimens (refer also to the EPMA results presented in Section C).

The Fe-20Cr alloys show a closed nitrided layer only after 5 hours of nitriding. This suggests the occurence of an incubation time. Additional nitriding experiments performed on Fe-20Cr alloys for less than 5 hours of nitriding at 580 °C showed that the nitriding process starts at isolated locations at the sample surface. At these locations, then, the discontinuously transformed microstructure, as shown in Figure 5(d) for a nitriding time of 7 hours, can already be observed.

The lamellar morphology of the microstructure after discontinuous coarsening is exhibited by Figure 7. The SEM micrograph in Figure 7(b) shows the occurrence of "subgrains" within a single original grain, characterized by different orientations of lamellae colonies.

Two trends can be indicated for the discontinuous coarsening reaction in dependence on the Cr content.

(1) The amount of discontinuously transformed areas increases with the chromium content of the alloy. Whereas the nitrided zones of the Fe-4Cr and Fe-7Cr alloys have only partially transformed discontinuously, the nitrided zones of the Fe-13Cr and Fe-20Cr alloys have experienced fully the discontinous coarsening.

(2) All discontinuously transformed grains of the nitrided Fe-4Cr alloy show a lot of subgrains (Figure 7(b)). The discontinuously transformed grains of the nitrided Fe-13Cr and Fe-20Cr alloys show only a few orientations for the lamellae colonies (Figures 5(c) and (d) and compare with Figure 5(a)). In this context, the nitrided Fe-7Cr alloy takes an intermediate position.

Upon performing additional nitriding experiments with Fe-20Cr *single crystals*, the same type of discontinuous coarsening morphology occured as observed for the Fe-20Cr polycrystals, except that, obviously, no grain boundaries occurred (Figure 8).

C. Concentration-Depth Profiles; EPMA

The nitrogen concentration-depth profiles of the Fe-7Cr alloy nitrided for 7 hours at 580 °C and of the Fe-20Cr alloy
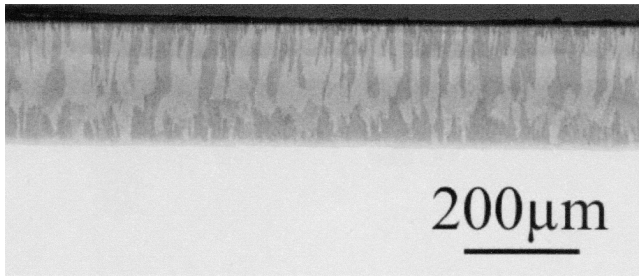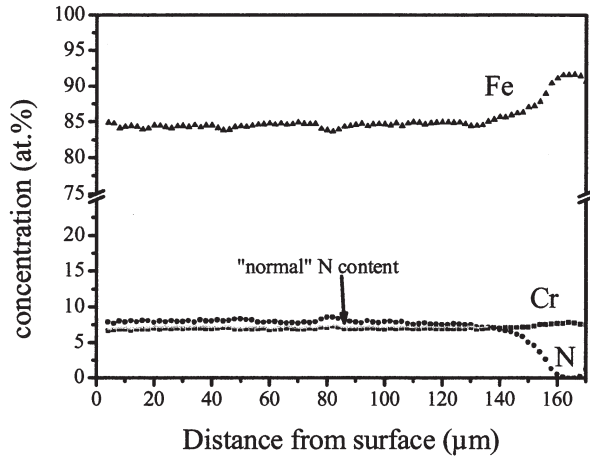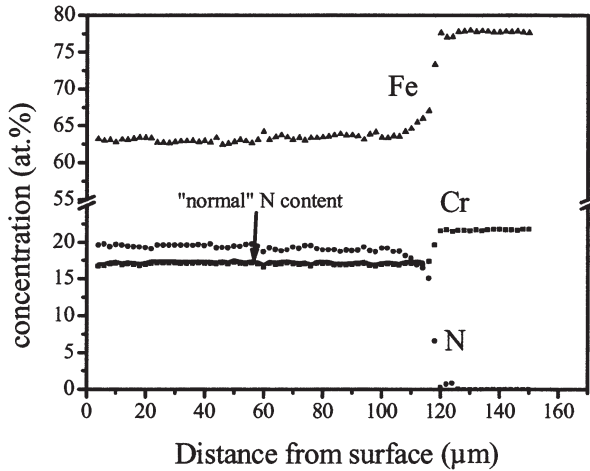
Fig. 8—Light micrograph of the cross section of a nitrided Fe-20Cr alloy single crystal nitrided at 580 °C with a nitriding potential of $r_n = 0.1$ atm$^{-1/2}$ for 48 h.
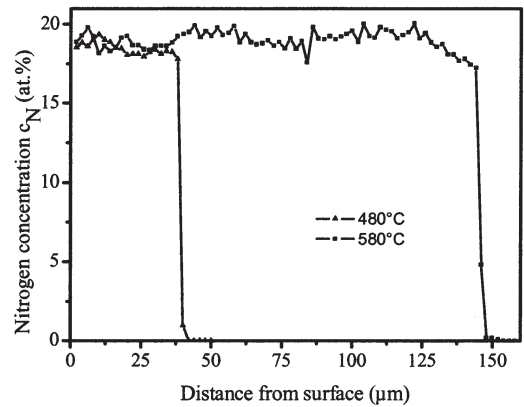

Fig. 10—Nitrogen-concentration depth profiles of Fe-20Cr alloys, as measured from cross sections by EPMA, nitrided for 24 h at 480 °C (gray dots) and for 24 h at 580 °C (black dots).

Fig. 9—The N, Fe, and Cr concentration-depth profiles as measured from cross sections by EPMA: (a) Fe-7Cr alloy nitrided for 7 h at 580 °C and (b) Fe-20Cr alloy nitrided for 15 h at 580 °C.

nitrided for 15 hours at 580 °C are presented in Figure 9. The EPMA results obtained for all alloys reveal an almost constant nitrogen level (plateau) in the nitrided region. Evidently, the higher the chromium content, the larger the nitriding time to reach a similar nitriding depth (*cf.* Figures 9(a) and (b)). The occurrence of a discontinuously transformed region in the nitrided zone does not influence the nitrogen concentration profile; thus, regions (1) and (2) discussed in

Section B cannot be distinguished in the concentration-depth profiles. The region where the nitrogen concentration decreases more or less gradually to zero corresponds to the transition from nitrided zone to non-nitrided core: region (3), as indicated in Section B, where the visibility of the grain boundaries gradually disappears in the optical micrographs. The width of this region overall decreases with increasing chromium content (*cf.* Figures 9(a) and (b)); it does not depend on the nitriding time. The average width of this transition zone (3) is 31 μm for Fe-4Cr, 24 μm for Fe-7Cr, 8 μm for Fe-13Cr, and 13 μm for Fe-20Cr.

It is important to note that the mass ratios of iron and chromium in the nitrided layer and in the non-nitrided core, as determined with EPMA, are equal. The change in the (relative) iron and chromium contents across the transition region (3) is only caused by the decrease of the nitrogen content from the nitrided case to the non-nitrided core. Hence, (long-range) diffusion of chromium and iron is negligible under the applied nitriding conditions.

The EPMA analysis of all nitrided specimens shows that the nitrogen concentration in the nitrided zone is larger than compatible with (1) the precipitation of all chromium as CrN, and (2) the equilibrium solubility of nitrogen in the (remaining) ferrite matrix (data in References 4 and 5). The normal amount of nitrogen (according to (1) and (2)), which should be present in the nitrided zone if no excess nitrogen occurs (Sections 1 and 2), is denoted by the gray lines (arrow) in Figure 9. Hence, excess nitrogen occurs in the nitrided zone. The "excess nitrogen" is thought to originate partly from the nitrogen attached to (*i.e.*, adsorbed at) the (submicroscopical) nitride platelets in the matrix and partly from dissolved nitrogen in the ferrite matrix strained by the misfit between the (submicroscopical) nitride platelets and the matrix, according to the model described in Reference 12. The normal content of N in the nitrided zone (*i.e.*, the amount of N comparable with precipitation of all Cr as CrN and the equilibrium solubility of nitrogen in the remaining ferrite matrix) has been indicated (arrows in Figure 9).

The influence of the nitriding temperature on the kinetics is shown in Figure 10. The larger penetration depth at higher temperatures is ascribed to two effects (*cf.* Eqs. [1] and [2]). First, obviously, the diffusion coefficient of nitrogen increases with increasing temperature. Second, and this is not always recognized, the solubility product K_{MeN_n} normally increases
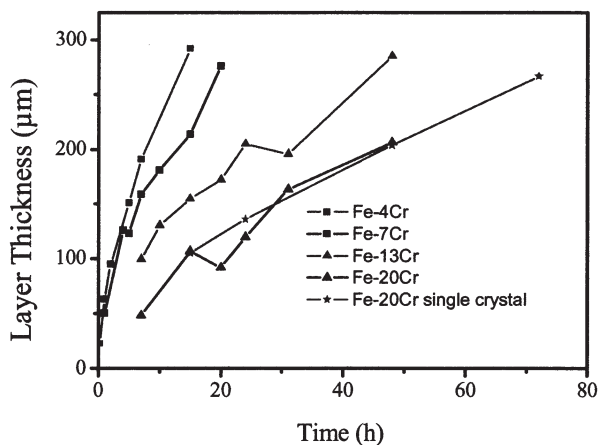
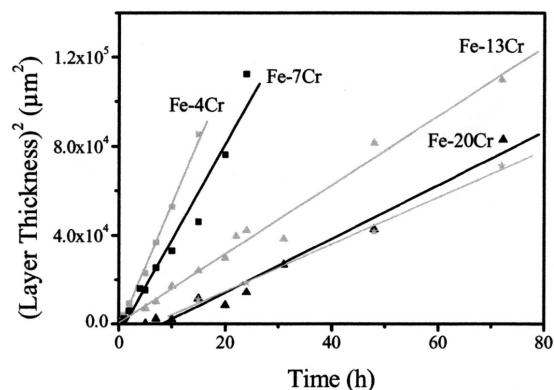Fig. 11—Thickness increase of the nitrided zone in dependence on the nitriding time and the Cr content.

Fig. 12—The squared nitrided layer thickness as a function of the nitriding time. The straight lines shown are least-squares fits to the data of the alloy concerned.

with increasing temperature, which leads to a $c_{N_\alpha}^s$ value increasing with temperature and thus a nitrogen-concentration gradient (in the ferrite matrix) increasing with temperature.

The determination of the thickness of the nitrided layers was performed applying light optical micrographs and nitrogen-concentration depth profiles obtained by EPMA analysis of the sample cross sections.

As discussed in Section B, the nitrided layers of the Fe-13Cr and Fe-20Cr alloys were completely discontinuously transformed. Therefore, the nitrided layer and the non-nitrided core can be distinguished very well in optical micrographs (Figures 5(c) and (d)) of the sample. The border between the nitrided layer and the non-nitrided core of the Fe-4Cr and Fe-7Cr alloys is not clearly visible in optical micrographs (see Figures 5(a) and (b)). Therefore, the nitrided layer thicknesses of the Fe-4Cr and Fe-7Cr alloys were determined from the nitrogen-concentration depth profiles. The nitrided layer thickness was taken as the depth where the nitrogen content (in the transition zone) equals half of the Cr content present in the alloy.

The thickness increase of the nitrided zone in dependence on the nitriding time and the Cr content at 580 °C is shown in Figure 11. The Cr content in the sample has a pronounced influence on the growth kinetics of the nitrided zone: the higher the Cr content, the smaller the layer thickness. Additionally, the thickness increase as a function of time is shown for nitrided Fe-20Cr single crystals (stars in Figure 11). The results for the Fe-20Cr single crystal are practically identical to those of the polycrystalline Fe-20Cr material, indicating that the presence of grain boundaries does not have a decisive influence on the growth kinetics of the nitrided zone. The contribution of nitrogen diffusion along grain boundaries can therefore be neglected for the growth of the nitrided zone.

V. ANALYSIS OF NITRIDING KINETICS

A. *Application of the Analytical, Approximate Model (Eq. [1])*

According to Eq. [1], plotting the squared layer thickness *vs* nitriding time should yield a straight line. Indeed the present experimental data show this behavior (Figure 12). The slope of the straight lines is given by $\dfrac{2 \cdot c_N^s \cdot D_N}{c_{Cr}}$ (*cf.* Eq. [1]).

Table III. Nitrogen Solubility in the Iron Matrix at the Surface, $c_{N_\alpha}^s$, as Obtained by Fitting Eq. [1] to the Experimental Data and As Obtained by EPMA from the Time-Dependent Experiments at 580 °C

Alloy	Fe-4Cr	Fe-7Cr	Fe-13Cr	Fe-20Cr
$c_{N_\alpha}^s$ from straight line fit (at. pct)	0.30	0.39	0.26	0.31
$c_{N_\alpha}^s$ from EPMA measurements (at. pct)	0.6	1.8	3.8	3.3
Incubation time (h)	0.5	0.4	1	7.12

Using literature data for D_N and the known chromium content of the alloy considered, values for $c_{N_\alpha}^s$ can be derived from the slopes. The diffusion coefficient of N in α-Fe at 580 °C is 1.14×10^{-11} m^2/s;[41] the data for c_{Cr} have been given in Section III–A. The thus obtained values for $c_{N_\alpha}^s$ are shown in Table III. They can be compared with the $c_{N_\alpha}^s$ values as obtained experimentally by EPMA (obtained as average values from the (first) three data points closest to the surface, after subtracting the amount of nitrogen contained in CrN from the total measured N concentration). Furthermore, Table III shows the incubation time obtained from the intercept of the fitted straight line with the time axis.

The equilibrium solubility of nitrogen in stress-free ferrite at 580 °C and $r_n = 0.1$ (atm$^{-1/2}$), $c_{N_\alpha}^{s,0}$, equals 0.24 at. pct,[5] which is lower than the $c_{N_\alpha}^s$ values for dissolved nitrogen at the surface as determined from the straight line fits in Figure 12. This suggests the presence of mobile excess N, which contributes to the growth of the nitrided layer (*cf.* Section II). Further, the values of the surface nitrogen content measured by EPMA are much higher than the values for *dissolved* nitrogen at the surface, determined by the straight line fits in Figure 12 according to the analytical model. This (already) suggests the presence of immobile excess nitrogen (nitrogen which is trapped and therefore cannot contribute to the growth of the nitrided layer, *cf.* Section II). It is essential to recognize that the $c_{N_\alpha}^s$ values determined from the straight line fits according to Eq. [1] and by fitting the numerical model (Section V–B) do *not* incorporate the contribution of immobile excess nitrogen.
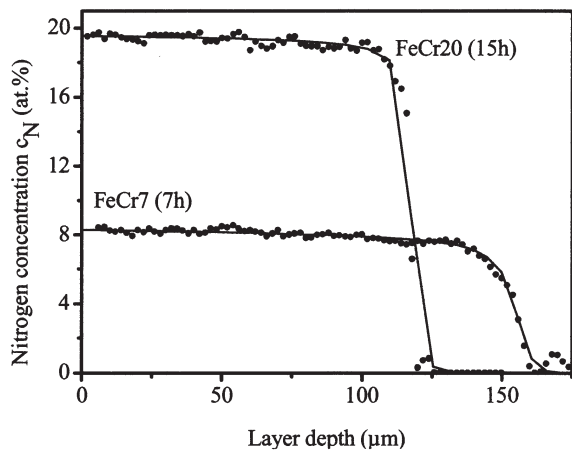
Fig. 13—Nitrogen-concentration profiles of nitrided Fe-7Cr and Fe-20Cr alloys, as measured with EPMA (black dots) and as calculated profiles (full lines) by the numerical model applying the parameters: $c_{N_\alpha}^s = 0.35$, $b = 1.18$, and $K_{CrN} = 0.02$ nm^{-6} for Fe-7Cr; and $c_{N_\alpha}^s = 0.26$; $b = 1.18$; and $K = 0.02$ nm^{-6} for Fe-20Cr.

B. Application of the Numerical, Rigorous Model (Eqs. [2] through [5])

Numerically calculated nitrogen depth profiles, according to Eqs. [2] through [6] and Figure 1, were fitted to experimentally determined nitrogen-depth profiles. The fitting parameters are K_{CrN}, $b = n + x$ (with $n = 1$) and $c_{N_\alpha}^s$ (cf. Section II). A two-step fitting procedure has been applied for the nitrogen-depth profiles measured at 580 °C.

The nitrogen-depth profiles have been first fitted individually. The solubility product K_{CrN} should not depend on nitriding time and Cr content at constant temperature. Accordingly, the average value of K_{CrN} ($K_{CrN} = 0.02$ nm^{-6}) has then been used as a constant in the second, definitive fitting, where only $c_{N_\alpha}^s$ and b were fit parameters. Examples of thus fitted nitrogen-concentration profiles are shown in Figure 13. The results obtained for the surface nitrogen content $c_{N_\alpha}^s$ and the nitride-particle composition parameter b have been gathered in Figure 14 and Table IV.

It follows from Figure 14 that in the case of the Fe-4Cr and Fe-7Cr alloys, the surface nitrogen content increases with nitriding time until a saturation level has been reached, whereas the surface nitrogen content of the Fe-13Cr and Fe-20Cr alloys appears to be independent of the nitriding time. Note that to achieve the same nitriding depth, much larger nitriding times are necessary for the Fe-13Cr and Fe-20Cr alloys than for the Fe-4Cr and Fe-7Cr alloys (Figure 14). The initial increase of $c_{N_\alpha}^s$ (as observed in Figure 14(a) for the Fe-7Cr and Fe-4Cr alloys) may be due to the finite period of time necessary to establish local equilibrium, at the surface of the substrate, of the gas atmosphere with the solid substrate. This effect has been observed for the nitriding of pure iron and is due to the finite rate of dissociation of NH$_3$.[42,43] The effect can be stronger for Fe-Cr, because in the presence of Cr, much more N has to be taken up before saturation at the surface has been attained. The solid horizontal lines in Figure 14 represent the average values of the surface nitrogen content as determined from all nitriding times; for the Fe-4Cr and Fe-7Cr alloys, only values of samples that were nitrided longer than 4 hours were considered to calculate
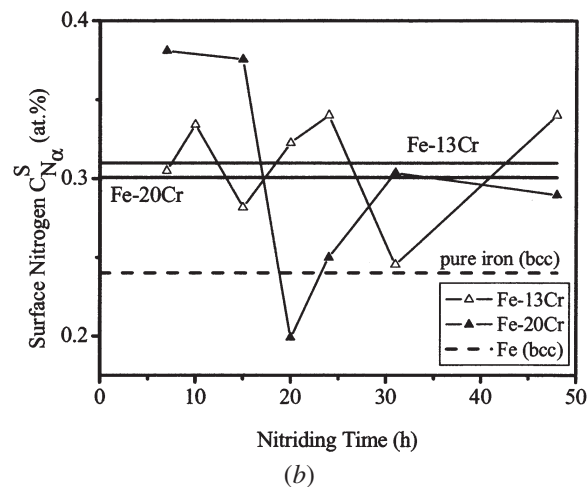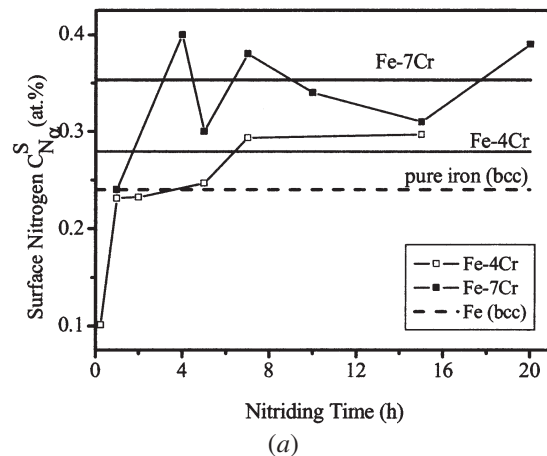

(a)

(b)

Fig. 14—Surface nitrogen concentration, $c_{N_\alpha}^s$, as a function of nitriding time, as result of fitting of the kinetic model described in Section II: (a) Fe-4Cr and Fe-7Cr alloys and (b) Fe-13Cr and Fe-20Cr alloys. The full horizontal lines represent the average C_N values for the alloys indicated (for the Fe-4Cr and Fe-7Cr alloys, only, values with a nitriding time larger than 4 h have been considered). The dashed horizontal lines in both figures indicate the nitrogen solubility of (unstrained) pure iron (bcc) at the applied nitriding conditions.

Table IV. Average values for $b = n + x = 1 + x$ and $c_{N_\alpha}^s$ in Dependence on the Cr Content for Nitriding at 580 °C*

Alloy	Fe-4Cr	Fe-7Cr	Fe-13Cr	Fe-20Cr
$c_{N_\alpha}^s$ (at. pct)	0.27	0.35	0.31	0.32
b	1.06	1.18	1.15	1.11

*In the case of the alloys with 4 and 7 wt pct Cr, only the values that were obtained from nitriding times larger than 4 h were considered.

the average value of $c_{N_\alpha}^s$, as for smaller times, no saturation at the surface occurs (cf. preceding discussion). To determine the $c_{N_\alpha}^s$ values of the Fe-20Cr alloys, an incubation time of 5 hours was accounted for (also Figure 12). This incubation time was determined by metallographical investigation of the cross sections of the nitrided zones. Fe-20Cr alloys nitrided shorter than 5 hours do not show a closed nitrided zone (cf. Section B). The dashed horizontal lines in Figure 14 denote the solubility of nitrogen in the unstrained α-Fe matrix calculated according to Reference 5.

After saturation with dissolved N has been realized upon nitriding at 580 °C, the solubility of nitrogen in the pure iron matrix of the nitrided Fe-Cr alloys is higher than as expected for pure iron (0.24 at. pct[5]). This indicates the presence of *mobile* excess nitrogen (*i.e.*, dissolved nitrogen) that contributes to the (further) growth of the nitrided zone. The average $c_{N_\alpha}^s$ values are presented in Table IV. It should be recognized that the quantitative subdivision of the amount of excess nitrogen in mobile and immobile excess nitrogen does not directly depend on the absolute accuracy of the total N content measured by EPMA: The amount of mobile excess nitrogen content, as determined by fitting, depends not in the first place on the level of N content, but depends largely on the depth of the nitrided zone (a change of only 0.04 at. pct mobile N leads to a change of nitriding depth of about 10 μm [also Figure 2], which is very well experimentally determinable); the much larger amount of immobile excess nitrogen then makes up for the remaining much larger part of the excess nitrogen.

The *b* values for all alloys show, just as the $c_{N_\alpha}^s$ values for the Fe-13Cr and Fe-20Cr alloys (Figure 14 and preceding discussion), no systematic dependence on nitriding time. Therefore, the time average values of *b* are shown in Table IV as a function of Cr content. Clearly, $b > 1$, which indicates the presence of *immobile* excess nitrogen in the nitrided zone.

Two explanations for this immobile excess nitrogen may be given.

(1) It may be suggested that this immobile excess N is due to N (originally) adsorbed at the faces of the submicroscopical, coherent nitride particles. At a later stage of nitriding, where practically the whole, or large parts of, the nitrided zone have experienced the discontinuous coarsening reaction, this N may no longer be accommodated at the interface of the CrN (now lamellae) with the α-Fe (now lamellae), and thus, this N could have segregated (*e.g.*, at grain boundaries) leading to porosity (N$_2$ formation), as has been detected.[23] Also then, this N cannot contribute to further nitriding and is accounted for in the kinetic model as immobile nitrogen.

(2) In earlier work on nitrided Fe-Cr,[12,14,32] it has been concluded that in the case of CrN in α-Fe (and in contrast with, *e.g.*, TiN in α-Fe or VN in α-Fe), no nitrogen adsorbs at the faces of the coherent CrN platelets. Further, as compared with the data for $c_{N_\alpha}^s$ obtained here, a much higher value of dissolved excess N has been deduced for an α-Fe matrix containing only submicroscopical, coherent CrN platelets: $c_{N_\alpha}^s$ values more than 3 times larger than the equilibrium solubility for α-Fe occur.[12,14] The present, much lower values for mobile excess N suggest that the largest part of this originally mobile excess N is no longer dissolved in the α-Fe matrix upon continued nitriding (note the pronounced extent of the discontinuous coarsening; previously discussed) and could have segregated (discussed further under explanation (1)). Thereby this part of the excess nitrogen is accounted for in the kinetic model as immobile nitrogen.

It must be remarked that if a certain solubility of Fe in CrN would occur (but evidence for this effect, under the nitriding conditions considered, lacks), then this is reflected in the fitting of the model by an increase of the amount of immobile excess nitrogen and thereby leaves the kinetic analysis presented here unimpeded.

It is striking to observe that the highest mobile and immobile excess nitrogen concentrations occur for the Fe-7Cr alloy. This observation can be interpreted as follows. The occurrence of excess nitrogen is ascribed primarily to the presence of fine, more or less coherent, Cr nitride precipitates: large nitride/matrix interfacial area ("trapped" immobile excess nitrogen) and pronounced nitride/matrix misfit-strain fields (dissolved, mobile excess nitrogen). An increase of Cr content in principle leads to a more chromium-nitride precipitate phase, which, if all nitride would precipitate in the finely coherent manner indicated previously, would lead to an amount of excess nitrogen that increases with the chromium content of the alloy. However, the amount of grains that exhibit the discontinuous coarsening reaction (thought to be associated with lack of capacity for excess nitrogen uptake) also increases with Cr content (Figure 5). Thus, some optimum Cr content could be imagined that would give the highest amount of excess nitrogen. Apparently, for the present alloy series and the present nitriding conditions, the Fe-7Cr alloy provides such an optimum (*cf*. Figure 5(b)).

One may wonder that, in particular, for the Fe-13Cr and Fe-20Cr alloys, where the entire nitrided zone has experienced the discontinuous coarsening reaction, the analysis of the growth kinetics yet suggests the occurrence of a significant amount of mobile excess nitrogen that directly influences the growth kinetics. A possible explanation may be that not all Cr is incorporated in the CrN lamellae of the discontinuous precipitation microstructure: a part of the Cr in the specimen may still be present as submicroscopical coherent CrN particles in the remaining α-Fe matrix (α-Fe lamellae), implying, that the discontinuous coarsening did not occur for all Cr (in CrN), as has been confirmed by recent transmission electron microscopical analysis carried out by our group.[40]

VI. CONCLUSIONS

1. Upon nitriding ferritic Fe-Cr alloys, various precipitation morphologies can be observed:
   a. initial precipitation of submicroscopical, coherent CrN precipitates in a ferrite matrix, and
   b. followed by a discontinuous coarsening reaction, involving the development of a (coarse) CrN/α-Fe lamellae structure.
2. The morphology of the nitrided zone depends on the Cr content. The nitrided Fe-4Cr and Fe-7Cr alloys exhibit grains of high hardness containing the fine, dispersed CrN precipitates and, in particular, near the surface, grain of low hardness having experienced the discontinuous transformation. The nitrided zones of the Fe-13 and Fe-20Cr alloys are completely discontinuously transformed.
3. In the nitrided zone, "excess nitrogen" occurs, *i.e.*, more nitrogen has been taken up than necessary for all Cr to precipitate as CrN and necessary to establish the equilibrium solubility of nitrogen in the ferrite matrix.
4. The development of the nitrogen-concentration depth profile can be described well by a numerical diffusion model that recognizes the presence of
   a. immobile excess nitrogen (trapped nitrogen), and
   b. mobile excess nitrogen (dissolved in the ferrite matrix).

5. The mobile excess nitrogen has a pronounced influence on the nitriding depth (and has a marginal effect on the nitrogen content of the nitrided zone); the immobile excess nitrogen expresses itself primarily through the (higher) nitrogen content of the nitrided zone.

6. An optimum Cr content corresponding to the highest amount of excess nitrogen taken up can occur as the net outcome of two trends:

    a. increase of amount of nitride precipitate with increase of Cr contant, and

    b. increase of the extent of the discontinuous coarsening reaction with increase of Cr content.

REFERENCES

1. E.J. Mittemeijer, ed.: *Mater. Sci, Forum*, 1992, vols. 102–104.
2. N.A. Wriedt, R.H. Gocken, and R.H. Nafziger: *Bull. Alloy Phase Diagrams*, 1987, vol. 8, p. 355.
3. E. Lehrer: *Z. Lektrochem.*, 1930, vol. 36, p. 383.
4. E.J. Mittemeijer and J.T. Slycke: *Surf. Eng.*, 1996, vol. 12, p. 152.
5. E.J. Mittemeijer and M.A.J. Somers: *Surf. Eng.*, 1997, vol. 13, p. 483.
6. M.A.J. Somers and E.J. Mittemeijer: *Metall. Mater. Trans. A*, 1995, vol. 26A, pp. 57-74.
7. H. Du and J. Ågren: *Z. Metallkd.*, 1995, vol. 8, p. 522.
8. H. Du, J. Ågren, H. Du, and J. Ågren: *Metall. Mater. Trans. A*, 1996, vol. A27, pp. 1073-80.
9. L. Torchane, P. Bilger, J. Dulcy, and M. Gantois: *Metall. Mater. Trans. A*, 1996, vol. 27A, pp. 1823-35.
10. K.H. Jack: *Proc. Conf. on Heat Treatment*, The Metals Society, London, 1975, p. 39.
11. B. Mortimer, P. Grieveson, and K.H. Jack: *Scand. J. Metall.*, 1972, vol. 1, p. 203.
12. M.A.J. Somers, R.M. Lankreijer, and E.J. Mittemeijer: *Phil. Mag.*, 1989, vol. 59, p. 353.
13. Y. Imai, M. Tsuyoshi, and M. Keikichi: *Sci. Rep. Res. Tohoku*, 1967, vol. A19, p. 35.
14. P.M. Hekker, H.C.F. Rozendaal, and E.J. Mittemeijer: *J. Mater. Sci.*, 1985, vol. 20, p. 718.
15. Y. Imai, T. Masumoto, and K. Maeda: *Sci. Rep. Res. Inst., Tohoku Univ. Ser. A—Phys., Chem. and Metall.*, 1967, vol. 19(1), p. 21.
16. K. Frisk: *Metall. Trans. A*, 1990, vol. 21A, pp. 2477-88.
17. D.B. Williams and E.P. Butler: *Int. Met. Rev.*, 1981, vol. 26, p. 153.
18. V.G. Permyakov, A.V. Belotskii, and R.I. Barabash: *Metallofizika*, 1972, vol. 42, p. 102.
19. B.J. Lightfoot and D.H. Jack: *Proc. Conference on Heat Treatment 1973*, The Metals Society, London, 1975, pp. 59-65.
20. E.J. Mittemeijer, A.B.P. Vogels, and P.J. van der Schaaf: *J. Mater. Sci.*, 1980, vol. 15, p. 3129.
21. P.C. van Wiggen, H.C.F. Rozendaal, and E.J. Mittemeijer: *J. Mater. Sci.*, 1985, vol. 20, p. 4561.
22. N. Granito, H. Kuwahara, and T. Aizawa: *J. Mater. Sci.*, 2002, vol. 37, p. 835.
23. R.E. Schacherl, P.C.J. Graat, and E.J. Mittemeijer: *Z. Metallkd*, 2002, vol. 93, p. 468.
24. J.L. Meijering: *Advances in Material Research 5*, Wiley Interscience, New York, NY, 1971, p. 1.
25. C. Alves, J. de Anchieta Rodrigues, and A. Eduardo Martinelli: *Mater. Sci. Eng.*, 2000, vol. 279, p. 10.
26. M.H. Bigliari, C.M. Brakman, E.J. Mittemeijer, and S. van der Zwaag: *Phil. Mag.*, 1995, vol. 72A, p. 931.
27. D.H. Jack: *Acta Metall.*, 1976, vol. 24, p. 137.
28. H.H. Podgurski and F.N. Davis: *Acta Metall.*, 1981, vol. 29, p. 1.
29. D.S. Rickerby, S. Henderson, A. Hendry, and K.H. Jack: *Acta Metall.*, 1986, vol. 34, p. 1687.
30. M.M. Yang and A.D. Krawitz: *Metall. Trans. A*, 1984, vol. 15A, pp. 1545-54.
31. H.H. Podgurski, R.A. Oriani, and N.A. Davis: with Appendix by J.C.M. Li and Y.T. Chou: *Trans. TMS-AIME*, 1969, 245, p. 1603.
32. E.J. Mittemeijer, H.C.F. Rozendaal, P.F. Colijn, P.J. van der Schaaf, R.T. Furnée: *Proc. Conf. on Heat Treatment 1981*, Birmingham, United Kingdom, 1981, The Metals Society, London, 1983, p. 107.
33. J. Crank: *Mathematics of Diffusion*, Clarendon Press, Oxford, United Kingdom, 1975, p. 137.
34. K. Bongartz, D.F. Lupton, and H. Schuster: *Metall. Trans. A*, 1980, vol. 11A, pp. 1983-93.
35. K. Bongartz, W.J. Quadakkers, R. Schulten, and H. Nickel: *Metall. Trans. A*, 1989, vol. 20A, pp. 1021-28.
36. Y. Sun and T. Bell: *Mater. Sci. Eng.*, 1997, vol. 224A, p. 36.
37. M. Gouné, T. Belmonte, J.M. Fiorani, S. Chomer, and H. Michele: *Thin Solid Films*, 2000, vols. 377–378, p. 543.
38. JCPDS-International Centre for Diffraction Data: *PCPDFWIN*, 1999, Version 202.
39. J.L. Pouchou and F. Pichoir: *Recherche Aérospatiale*, 1984, vol. 3, pp. 167-92.
40. P. Zieba, R.E. Schacherl, and E.J. Mittemeijer: unpublished research.
41. J.D. Fast and M.B. Verrijp: *J. Iron Steel Inst.*, 1954, vol. 126, p. 24.
42. H.C.F. Rozendaal, E.J. Mittemeijer, P.F. Colijn, and P.J. van der Schaaf: *Metall. Trans. A*, 1983, vol. 14A, pp. 395-99.
43. P.B. Friehling, F.W. Poulsen, and M.A.J. Somers: *Z. Metallkd.*, 2001, vol. 92, p. 589.